Journal of High Energy Physics, Gravitation and Cosmology, 2026, 12(1), 585-605
https://www.scirp.org/journal/jhepgc
ISSN Online: 2380-4335
ISSN Print: 2380-4327

Stimulated Emission of Gravitational Waves via Dissimilar Superconducting Josephson Junctions

Gary V. Stephenson

Seculine Consulting, Cupertino, CA, USA
Email: seculine@gmail.com

How to cite this paper: Stephenson, G.V. (2026) Stimulated Emission of Gravitational Waves via Dissimilar Superconducting Josephson Junctions. *Journal of High Energy Physics, Gravitation and Cosmology*, **12**, 585-605.
https://doi.org/10.4236/jhepgc.2026.121029

Received: December 29, 2025
Accepted: January 26, 2026
Published: January 29, 2026

Abstract

An experiment is proposed to prove the stimulated emission of gravitational waves is experimentally possible. The proposal suggests that Josephson Junctions with dissimilar superconductors, an s-wave joined to a d-wave, can force spin 2 transitions, triggering the emission of gravitational waves.

Keywords

Gravitational Waves, GASER, Superconductors, Josephson Junctions

1. Introduction

An approach to the quantum emission of gravitational waves is described, along with a suggested experiment.

Semi-classical approaches covered in this paper include details gleaned from these important historical references:

Section 2.0, 1964 Halpern & Laurent, "On the Gravitational Radiation of Microscopic Systems".

Section 3.0, 1982 Ford, "Gravitational Radiation by Quantum Systems".

Section 4.0, 2012 Fontana, "High Temperature Superconductors as Quantum Sources of Gravitational Waves: The HTSC GASER".

After review of this historical supporting literature an experimental approach is proposed in Section 5.0.

2. Halpern & Laurent's "On the Gravitational Radiation of Microscopic Systems"

Leopold Ernst Halpern (1925-2006) was an Austrian-born theoretical physicist

best known for his work on gravitation, especially attempts to generalize Einstein's general relativity by incorporating spin and the de Sitter group into the fundamental structure of spacetime. He was closely associated with both Erwin Schrödinger and Paul Dirac and later became a long-time member of the gravitational physics community in the United States, particularly at Florida State University and in connection with the Gravity Probe B experiment [1].

One of his earlier works was Halpern and Laurent (1964), "On the Gravitational Radiation of Microscopic Systems" [2], which later came to the attention of researcher Giorgio Fontana [3]. This paper forms the introductory material describing predicted radiation patterns and strengths for gravitational emissions triggered from spin 2 transitions in a suitable solid-state material. In it Halpern and his co-author Laurent:

Developed the theory describing the emission of gravitational radiation from quantum systems.

Applied the linearized theory of gravitational radiation to quantum systems.

Calculated gravitational quadrupolar transitions permitted for the emission of gravitons.

Compared the emission of gravitons to the emission of photons, showing that the spontaneous emission of gravitons from quantum systems is comparatively small due to the weakness of gravity.

Halpern's approach was largely semi-classical but was later extended to a more fully quantum approach by Ford in 1982 [4], and will be summarized in Section 2 of this paper.

Halpern's subsequent work also suggested the possibility of a "GASER" (gravitational counterpart of a laser) using stimulated emission. The concept of a GASER was expanded on by Fontana [3] and will be summarized in Section 3 of this paper.

For the purposes of the present section, the most relevant material regarding predicted gravitational radiation is drawn from [2], the angular distribution of electromagnetic and gravitational multipole radiation

of the lowest orders, the gravitational transitions of which are reproduced below:

Gravitational radiation for $J = 2$, $l = 0$:

$$\text{Angular dependence } \vec{\mathcal{Y}}^{\theta,\varphi}_{J,l,M} \text{ of the potentials: } \sqrt{\frac{1}{4\pi}}\overrightarrow{\omega_M} \tag{1}$$

Angular dependence of the amplitudes $\vec{\mathcal{Y}}^{\theta,\varphi}_{J,l,M}\cdot\overline{\omega_{\mp 2}}$:

$$\text{For } M=2,\ \mu=+2,\ (4\pi)^{-\frac{1}{2}}\cdot\cos^4\frac{\theta}{2}\cdot\exp[2i\varphi] \tag{2}$$

$$\text{For } M=2,\ \mu=-2,\ (4\pi)^{-\frac{1}{2}}\cdot\sin^4\frac{\theta}{2}\cdot\exp[2i\varphi] \tag{3}$$

$$\text{For } M=1,\ \mu=+2,\ (\pi)^{-\frac{1}{2}}\cdot\cos^3\frac{\theta}{2}\cdot\sin\frac{\theta}{2}\cdot\exp[2i\varphi] \tag{4}$$

$$\text{For } M=1,\ \mu=-2,\ -(\pi)^{-\frac{1}{2}}\cdot\cos\frac{\theta}{2}\cdot\sin^3\frac{\theta}{2}\cdot\exp[2i\varphi] \tag{5}$$

$$\text{For} \quad M=0\,, \quad \mu=+/-2\,, \quad (6)^{-\frac{1}{2}}\cdot\cos^2\frac{\theta}{2}\cdot\sin^2\frac{\theta}{2} \tag{6}$$

Angular dependence of the total radiation: $\left|\vec{\mathcal{Y}}^{\theta,\varphi}_{J,l,M}\cdot\overline{\omega_{+2}}\right|^2+\left|\vec{\mathcal{Y}}^{\theta,\varphi}_{J,l,M}\cdot\overline{\omega_{-2}}\right|^2$:

$$\text{For} \quad M=2\,, \quad \cos^8\frac{\theta}{2}\cdot\sin^8\frac{\theta}{2} \tag{7}$$

"*Gravitational radiation for* $J=2$, $l=1$:

Angular dependence of the potentials:

$$\text{For} \quad M=2\,, \quad (2\pi)^{-\frac{1}{2}}\cdot\left(\cos\theta\cdot\overrightarrow{\omega_2}+\frac{1}{2}\sin\theta\cdot\exp\left[2i\varphi\right]\overrightarrow{\omega_1}\right) \tag{8}$$

Angular dependence of the amplitudes:

$$\text{For} \quad M=2\,, \quad \mu=+2\,, \quad (2\pi)^{-\frac{1}{2}}\cdot\cos^4\frac{\theta}{2}\cdot\exp\left[2i\varphi\right] \tag{9}$$

$$\text{For} \quad M=2\,, \quad \mu=-2\,, \quad -(2\pi)^{-\frac{1}{2}}\cdot\sin^4\frac{\theta}{2}\cdot\exp\left[2i\varphi\right] \tag{10}$$

Angular dependence of the total radiation: the same as for $J=2$, $l=0$."

See Section 6.0 for a summary of the nomenclature used here. As admitted by the authors themselves in the **Appendix A** of [2], these predicted radiation patterns are the result of a linearized theory of gravitational radiation, and "The linearized equations are therefore not consistent, but they may nevertheless serve to evaluate the radiation field approximately" [2].

3. Ford's "Gravitational Radiation by Quantum Systems"

Lawrence H. Ford is a professor emeritus of physics at Tufts University, associated with the Department of Physics and Astronomy and the Tufts Institute of Cosmology.

He joined Tufts as an assistant professor in 1980, was promoted to associate professor in 1985, and became a full professor in 1992; he was later elected a fellow of the American Physical Society in 2004 for work in quantum field theory in flat and curved spacetime. Early in his tenure at Tufts, in 1982, he published "Gravitational Radiation by Quantum Systems" [4], the topic of this section.

As introduced in the abstract of Ford 1982 [4].

> "The limits of validity of the semiclassical theory in which gravity is unquantized is discussed. This is done by comparing the emission of classical gravitational waves in the semiclassical theory with graviton emission in quantum gravity theory. It is shown that these can be quite different even for macroscopic systems. Thus, quantum gravitational effects can manifest themselves on a macroscopic scale."

This paper has an interesting structure: Section II "Gravitational Radiation by Quantum Systems" was divided into a Part A, which treated the subject semi-classically, and a Part B, where the author contrasts the prior approach with a purely quantum theory. Part A, from [4], (13), the semi-classical case, the metric pertur-

bation $h_{\mu\nu}$ is summarized here in Equation (11).

$$\overline{h_{\mu\nu}} = \overline{h_{\mu\nu}^{in}} + 16\pi \int G_{r(X,\dot{X})} T_{\mu\nu(\dot{X})} \mathrm{d}^4 x' \tag{11}$$

where:

$\overline{h_{\mu\nu}}$ = metric perturbation

$\overline{h_{\mu\nu}^{in}}$ = in-field metric component

$G_r\left(X,\dot{X}\right)$ = retarded Green's function

$T_{\mu\nu}\left(\dot{X}\right)$ = energy momentum tensor

He concludes Section II Part B with an insightful comparison of the resultant integrated energy-momentum tensors from both approaches:

"The essential difference between the semiclassical and the quantum results is that the [semi-classical case] depends upon a product of expectation values whereas [quantum case] depends upon an expectation value of products."

The example of a scalar field source was then explored for comparative purposes in section III of this same reference [4] to explore what would happen if the two approaches were set equal. Reference [4] Equation (27) embodies the above quoted comparison by setting the two approaches equal, reproduced as Equation (12) here.

$$\left\langle T_{\mu\nu}\left(\dot{X}\right)\right\rangle \left\langle T_{\alpha\beta}\left(\ddot{X}\right)\right\rangle = \left\langle T_{\mu\nu}\left(\dot{X}\right)\cdot T_{\alpha\beta}\left(\ddot{X}\right)\right\rangle \tag{12}$$

where:

$T_{\mu\nu}\left(\dot{X}\right)$ = energy momentum tensor

$T_{\alpha\beta}\left(\ddot{X}\right)$ = energy momentum tensor perturbation

But the author does not stop there; he goes on to compare the predicted gravitational wave (GW) power radiated in the semi-classical case P_{sc}, with a predicted power in the quantum case, P_q.

Radiated power in semi-classical theory (P_{sc}) is given in [4] [5], and reproduced here is in Equation (13):

$$P \approx P_{sc} = \lceil z \rceil^4 \omega^4 \left(\omega\ell\right)^{-\alpha} \approx \varepsilon^2 \omega^2 \ell^6 \left(\omega\ell\right)^{-\alpha} \tag{13}$$

where:

$P \approx P_{sc}$ = semi-classical radiated power

$\lceil z \rceil$ = resonant cavity dimension

ω = radiating frequency

ℓ = characteristic cavity dimension

ε = average energy density in the cavity

α = scaling constant, where $\left(\omega\ell\right)^{-\alpha}$ is mode function

As contrasted with radiated gravitational wave power from quantum theory (P_q) is given by [4] reproduced here as Equation (14):

$$P_q = n^2 \omega^4 \left(\omega\ell\right)^{-\alpha} \tag{14}$$

where:

P_q = quantum case radiated power

ω = radiating frequency

ℓ = characteristic cavity dimension

β = quantum scaling constant

n = number of quantum radiators

Noting that "n" can be made arbitrarily large, Ford concluded that the difference should be measurable, were there a way to emit and measure GW power levels in a laboratory setting [4].

In Sections 3 and 4 we'll explore the proposals to do just that, which unfortunately very likely depend solely on the second approach being the correct one.

4. Fontana's "High Temperature Superconductors as Quantum Sources of Gravitational Waves"

4.1. Historical Background

The works of Halpern & Laurent [2] and Ford [4] subsequently caught the attention of an Italian engineering researcher Giorgio Fontana at the University of Trento [3]. Fontana had been involved in the design of the Silicon Vertex Tracker (SVT) for the proposed SuperB experiment. SuperB was a proposed high-luminosity electron–positron collider and B-factory experiment, designed to study B mesons and search for CP violations. Cancelled in 2012, it would have been an asymmetric electron–positron collider (electrons at 7 GeV, positrons at 4 GeV) operating at the $\Upsilon(4S)$ resonance, where $B\text{-}\bar{B}$ pairs are copiously produced.

The SVT for the proposed SuperB experiment was designed to meet extremely challenging requirements imposed by the accelerator's target of achieving a luminosity 100 times greater than its predecessor, the BaBar experiment.

The SuperB SVT design was largely based on the successful BaBar 5 layer SVT but featured a crucial upgrade: the addition of a new, ultra-precise innermost layer, called Layer 0, to compensate for the reduced boost in the new collider's asymmetric beam energies, the innermost closest to the Interaction Point, resulting in an SVT with a total of 6 layers.

4.2. The GASER Application

Fontana's insight was that a similar multilayer design might also be advantageously applied to the problems of GW detection and emission, including the GASER as described in reference [2]. This led Fontana to publish a series of papers on the topic, culminating the publication of "High Temperature Superconductors as Quantum Sources of Gravitational Waves: The HTSC GASER" in 2012 [3]. All quantum detectors and emitters operate via orbital energy transitions, and Fontana realized that certain spin 2 transition could help force graviton emissions. Quoting from the abstract to reference [3]:

> "…it is known from theory that electronic transitions between s and d states may produce the emission of gravitational waves. In normal materials, s-d transitions are suppressed by competing electric and magnetic transitions that have much higher probabilities; this is not the case of Cooper pairs in HTSC, which cannot support states other than s-wave or d-wave. To give

theoretical foundations to a potential technology capable of constructing a quantum source of gravitational waves, this paper will also discuss means for creating coherence and population inversion and means to increase [graviton] emission probability."

Examples of photon and graviton transitions are depicted in Figure 1, where photon transitions are blue, and graviton transitions are depicted in red. For a GASER, the ideal emission junction would favor spin 2 graviton emitting transitions over spin 1 photon emitting transitions.

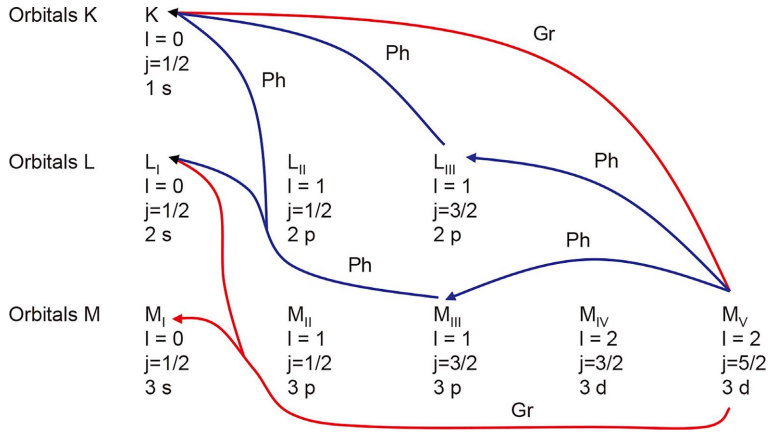

Figure 1. Examples of photon and graviton transmissions [3] (reprinted with permission).

4.3. Dissimilar Josephson Junctions (DJJs)

For the task of maximizing the population of spin 2 graviton transitions Fontana designed an s-wave to d-wave Josephson Junction. If biased appropriately it should invert the graviton emissions over the photon emissions. See the situation at the emission junction as depicted in Figure 2.

There is a subtlety in Figure 2: coherent transitions from s-wave to d-wave states are the important factor in forcing spin 2 transitions. Here the "s-states" and "d-states" refer to orbital angular momentum symmetries in the superconducting order parameter, not the band structure.

What is important for this pairing is to pair a superconductor with s-wave state pairing with a superconductor with predominately d-wave state pairing, with some s-wave state paring being acceptable. It is the s-wave to d-wave dissimilarity that is the important design feature in DJJs. This distinction will be discussed further in Section 5.2.

4.4. Emission Power Estimation

In the case of spontaneous decay, comparing the decay rate of graviton transitions Γ_g to those of electromagnetic dipole transitions Γ_e, one can cite for instance the value listed in Kiefer's 4th ed. of *Quantum Gravity*, Equation (2.60) [6], reproduced here as Equation (15):

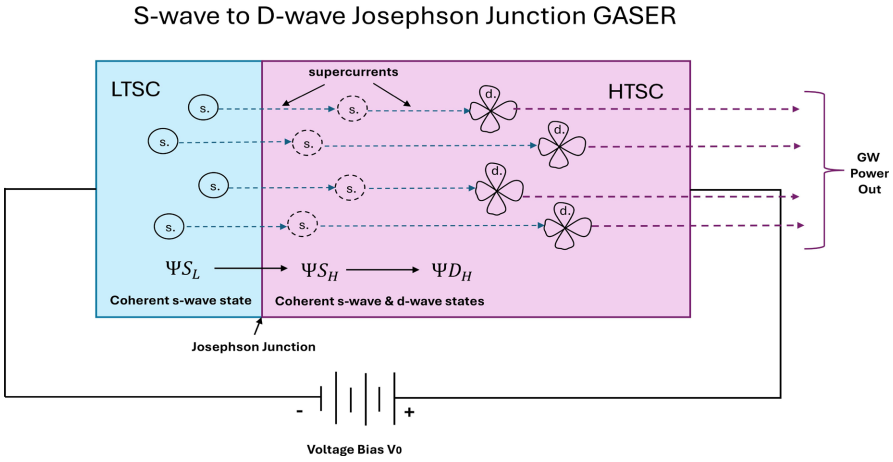

Figure 2. Graviton emissions at a s-wave to d-wave junction, adapted from [3].

$$\frac{\Gamma_g}{\Gamma_e} \approx 1.28 \times 10^{-47} \tag{15}$$

Which is less than encouraging. However, turning to the graviton emission probability in superconducting junctions, Fontana [3] pointed out that the emission ratio for matrix elements of equal structures is more on the order of $8\pi G m_e^2 / e^2$, which leads one to an emission probability of gravitons is $4.8 \cdot 10^{-43}$ times the emission probability of photons for the electron transition. Assuming Cooper pair density of $N = 10^{20}/\text{cm}^3$, with 10 cm^3 of material, wavefunction coherence can amplify the probability of gravitons emission to the level of typical spontaneous photon emission in a single atom, the "ideal GASER" case. Fontana observed that "There are indeed $5 \cdot 10^{21}/\text{cm}^3$ elementary cells in YBCO" [5].

Coherence gain is n^2, where n is the number of emitters, because the individual emitters add together in phase, and the resulting intensity is proportional to the square of the resultant field emission.

While the upper emission bound will be limited by material saturation, Fontana [3] makes reference to Ford's [4] discussion surrounding Equation (48) in [4], based in part on L. P. Grishchuck and M. V. Sazhin [5], to point out quantum gravity effects can be macroscopically large. See below for an extract from [4]:

"It is sometimes stated that quantum gravity effects should be characterized by Planck dimensions. Yet in [some] examples discussed it is possible for quantum gravity effects to be macroscopically large. The resolution of this apparent discrepancy can be found by examining results such as [Equation (14) above.] If we let $\omega \sim \ell$, then we can write this equation" [as (16)]:

$$\frac{P}{P_P} \approx n^2 \left(\frac{\omega}{\omega_p} \right)^4 \tag{16}$$

where:

P = emitted GW power

P_p = Planck power ~ 10^{-5}g/10^{-44}sec - 10^{60} ergs/sec

ω = emitted frequency

ω_p = Planck frequency ~10^{+44}/sec

ℓ = characteristic cavity dimension

n = number of quantum emitters

"Thus it is true that the result is characterized by Planck dimensions, except for the factor of n^2, which can be arbitrarily large. It is the presence of such large dimensionless numbers in the theory arising from the choice of quantum state which can produce quantum gravity effects on scales much larger than the Planck scale." [4]

Estimated GW emitted power out, and the estimated sensitivity to GW power inputs for Dissimilar Josephson Junctions, or DJJs, will be discussed in Sections 5.3 and 5.4, respectively.

5. Experiment Design Considerations

Thus far we've discussed only the generation and emission of High Frequency Gravitational Waves (HFGW) by DJJs, not their detection. However, as Fontana noted in [3], "It must be observed that reciprocity will permit the design and construction of HTSC GASERS pumped by HFGW instead of DC electric current." In other words, the same devices that can be biased to emit HFGW can also be used passively to detect them. This would be a necessary element of any laboratory test, for there is very little value in generating HFGW signals that cannot be detected. Whether the signals generated by DJJ technology are strong enough to be detected by that same technology is still an open question and will be treated in more detail in Section 4.3.

Then there is the matter of what device type should be chosen for an experimental setup. Fontana [3] suggested a bulk device, the conceptual design of which is depicted in **Figure 3**. In this particular diagram a capacitor bank 'C' supplies DC bias through a thyristor until the current drops below a holding level, at which point it switches off. There are two impracticalities associated with this design. The first is that since the DJJ includes LTSC material, the entire setup must be cooled to near absolute zero temperatures, which would require a very large and complex cryogenic cooling system. The second is that, while the LTSC could be lead (Pb), and may be vapor dispositioned, the device envisioned here would require bulk HTSC of a d-wave type, for instance YBCO, which is notoriously difficult and expensive to fabricate.

A more practical design might envision the use of thin films for both the s-wave superconductor (the LTSC) as well as the d-wave superconductor (the HTSC), ideally on a standard substrate such as silicon (Si). If one chose a standard size silicon wafer one could even envision testing such a thin film device in standard low temperature cryogenic probe stations, such as those used for existing quantum computing wafers. Leveraging existing quantum computing technology for the development of quantum gravitation devices would save an enormous amount of development costs. Design and material aspects of thin film device design con-

siderations will be examined in Sections 5.1 and 5.2.

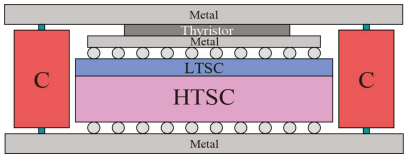

Figure 3. A bulk device experimental design for dissimilar josephson junctions [3] (reprinted with permission).

Finally, it would be remiss to not mention in passing the notion of focusing HFGW energy, to boost its power cross section, thereby improving detectability. In a laboratory or engineering setting, it is well known that matter cannot be fashioned into a useful gravitational wave lens the way glass or mirrors are used for light, because the coupling of gravitational waves to any realistic material is too weak to produce appreciable focusing [7]. Only astronomical-scale mass distributions produce noticeable lensing effects, and those are fixed by astrophysics rather than engineered devices.

However, it would be possible to fashion a curved array of emitters such that the wavefronts constructively interfere at a certain focal point. Such a point was made by Fontana [3] and in [8], and this idea is reproduced in **Figure 4**.

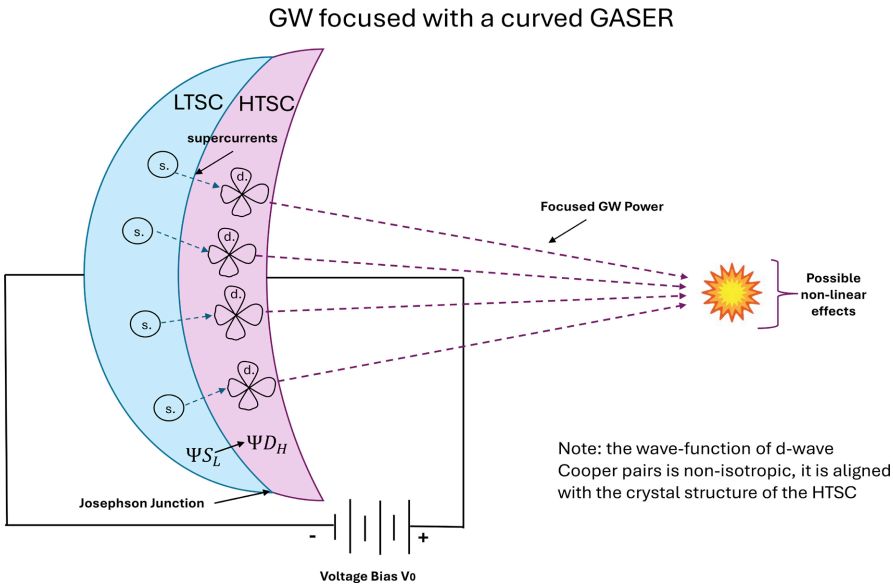

Figure 4. A curved GASER to create an HFGW focal point, adapted from [3] [8].

In the technological landscape of flat two-dimensional thin films, such a device would be tedious to engineer and expensive to build. Better in practice one might judge to replace the delta radii reflected in the curvature of **Figure 4** with delay times creating the same delay pattern as the curvature of the emitter array, as is commonly done in phased array communication antennae and radar arrays. Such

will be the impetus for the phased array design choices presented in Section 4.1.

5.1. Phased Array Emitters/Receivers Design

5.1.1. Operating Frequency Selection

Designing a thin film HFGW emitter begs the questions of how to achieve an AC oscillating signal, and what operating frequency should be chosen. On the topic of creating an AC signal, if one is using Josephson Junctions, we may leverage the AC Josephson Effect as reproduced in **Figure 5** [9].

Note that in the AC Josephson Effect the frequency at which the junction oscillates is related to the applied bias voltage $V0$. This is referred to the as the Josephson frequency, f_j. The higher the applied bias voltage, the higher the oscillation frequency.

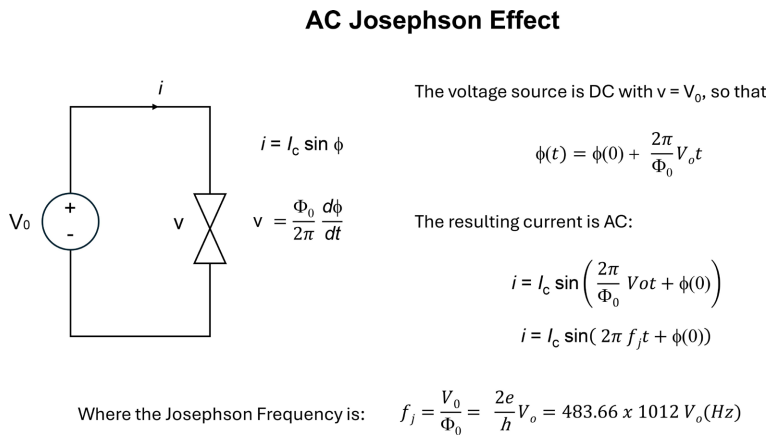

Figure 5. The AC josephson effect [9].

The next question becomes what operating frequency should be selected for an HFGW emission (&/or detection) device? A few considerations here might include what frequencies permit the use of standard technology, what frequencies are authorized for use, and what frequencies permit reasonably phased arrays of emitter geometries to be masked onto standard wafer sizes. These three factors were combined to generate **Table 1**, with the frequency judged as currently optimum to be highlighted.

Table 1. US Amateur microwave bands selected for examination [10].

Frequency (GHz)	Wavelength (cm)	Qtr wave geom (cm)	JJ operating voltage* (uV)
1.296	23.15	5.79	2.68
2.32	12.93	3.23	4.80
3.4	8.82	2.21	7.03
5.76	5.21	1.30	11.91
10.368	2.89	0.72	21.44
24.048	1.25	0.31	49.73

Continued

47.088	0.64	0.16	97.37
76.233	0.39	0.10	157.64
120	0.25	0.06	248.14
249	0.12	0.03	514.89
6250	0.0048	0.0012	12923.90

Table 1 was compiled based on amateur bands available for use in the USA [10]. In the case of this table 24 GHz was judged to be the optimum operating frequency because frequencies below this operating point had emitter features too large for a phased array to fit on a standard wafer size, and the use of frequencies above this operating point were judged to be too unwieldy to consider using standard state of the art microwave technology.

5.1.2. Pairing with Standard Wafer Sizes

We turn now to the problem of how to inscribe a thin film phased array of emitters, or receivers, onto a standard wafer size. The approach taken here is that the larger the wafer size, the larger and more effective the possible phased array. However, it is also the case that not every foundry can support every wafer size, so that there may be a practical limit to the largest size a particular foundry can accommodate. This situation is summarized in Table 2 [11].

Table 2. Standard electronics wafer sizes [11].

Wafer size	Typical thickness	Year introduced
1-inch (25 mm)		1960
2-inch (51 mm)	275 µm	1969
3-inch (76 mm)	375 µm	1972
4-inch (100 mm)	525 µm	1976
4.9 inch (125 mm)	625 µm	1981
150 mm (5.9 inch, usually referred to as “6 inch”)	675 µm	1983
200 mm (7.9 inch, usually referred to as “8 inch”)	725 µm	1992
300 mm (11.8 inch, usually referred to as “12 inch”)	775 µm	1999
450 mm (17.7 inch) (proposed)	925 µm	–
675-millimetre (26.6 in) (theoretical)	unknown	–

Wafer sizes are characterized in terms of their diameter, the most common of which are the 150 mm (6”) and the 200 mm (8”). In the next section possible phased array layouts for these two form factors are presented.

5.1.3. Phased Array Spacing Examples (150 mm, 200 mm Cases)

The layout approach taken for the HFGW phased array emitters (and detectors) is to create quarter wave emitter (& receiver) pads one quarter wavelength in diameter, for a nearly in phase wavefront, spaced by full wavelength increments to keep all emitters in phase. Example layouts are presented here for the 150 mm and 200 mm wafer sizes, see Figure 6(a) and Figure 6(b).

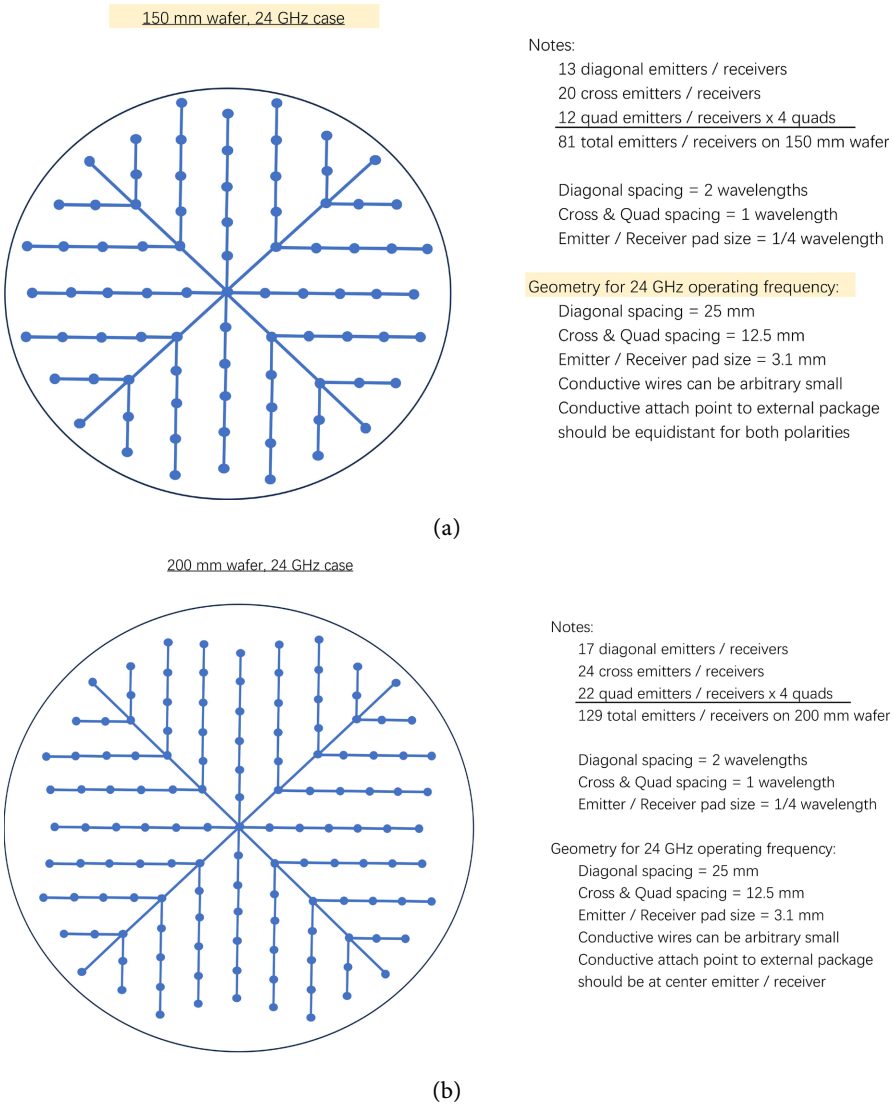

Figure 6. (a) Phased array layout example for 150 mm wafers; (b) Phased array layout example for 200 mm wafers.

Note that these example layouts create a flat wavefront, without a focal point. If a focal point is desired additional trace lengths may be added or subtracted for the appropriate delay lines to shape the wavefront.

5.2. Material Considerations

Turning now to material consideration for DJJ device fabrication, we may recall

here that in Fontana's work he suggests Pb/YBCO as a possible material paring choice for s-wave/d-wave junctions [3] [6]. While the development and production of Pb-curate Josephson junctions is considered settled art [12] [13], subsequent work has demonstrated that "high-temperature cuprate superconductors are among the most complex materials ever explored for practical application" [14]. Among the manufacturing challenges for cuprates one may list the following [14]-[16]:

- Cuprates are multicomponent oxides (e.g., Y–Ba–Cu–O, Bi–Sr–Ca–Cu–O) that must be synthesized at high temperatures (≈700˚C - 800˚C) with tight control of cation ratios and oxygen partial pressure to obtain the right superconducting phase.
- Some constituents (e.g., barium, bismuth, mercury, thallium) are volatile or reactive at processing temperatures, so loss, decomposition, or parasitic phases are common and can suppress Tc and current-carrying capability.
- High angle grain boundaries act as weak links that drastically reduce the critical current density in polycrystalline cuprates like YBCO and Bi 2212.
- Manufacturing must therefore create highly textured or near single crystal material (e.g., epitaxial films, biaxially textured substrates, melt textured bulks), which adds processing steps such as buffer layers, seed crystals, and careful thermal profiles.
- Superconductivity in cuprates is extremely sensitive to oxygen content; precise oxygen stoichiometry and doping require carefully controlled anneals in oxygen or mixed-gas atmospheres.
- For Bi-2212, high-pressure overpressure heat treatments (≈50 bar Ar/O2) are needed to densify filaments and optimize connectivity, but these processes are technically demanding and can cause leakage or failure.

All of the above detail is just to point out the desirability of avoiding the use of HTSC cuprates entirely if possible, thereby avoiding the variations and unknowns introduced by such a demanding material. As was discussed in Section 4.3, what's important at the Josephson Junction is creating an s-wave/d-wave junction. For a d-wave HTSC, only cuprates have exhibited this combination of properties. Therefore, with the current technology we have no choice but to select YBCO or a related cuprate for our HTSC material.

The s-wave trade space is examined in **Table 3**, where selected s-wave elemental superconductors are listed [17].

Table 3. List of elemental superconductors (selected s-wave choices) [17].

Substance	Class	T_C (K)	H_C (T)	Type	BCS
Al	Element	1.2	0.01	I	yes
Cd	Element	0.52	0.0028	I	yes
Ga	Element	1.083	0.0058	I	yes
α-Hg	Element	4.15	0.04	I	yes

Continued

β-Hg	Element	3.95	0.04	I	yes
In	Element	3.4	0.03	I	yes
Ir	Element	0.14	0.0016	I	yes
Mo	Element	0.92	0.0096	I	yes
Os	Element	0.65	0.007	I	yes
Pb	Element	7.19	0.08	I	yes
Re	Element	2.4	0.03	I	yes
Sn	Element	3.72	0.03	I	yes
Ta	Element	4.48	0.09	I	yes
α-Th	Element	1.37	0.013	I	yes
Tl	Element	2.39	0.02	I	yes

Although other choices and combinations are certainly possible, preliminary down selections for s-wave materials would be those highlighted here, most commonly lead (Pb), as suggested by Fontana [3], or one may substitute Tantalum (Ta), for those not willing to expose their deposition chamber to Pb.

5.3. Signal Power Approximations

In this section emission powers will be estimated, along with detection sensitivities, to determine whether these thin film devices may be sufficient for HFGW generation and detection in a laboratory setting. The experimental setup under analysis is depicted in Figure 7. We assume here the choice of Pb for the s-wave SC, and YBCO for the d-wave SC. The operating temperature will need to be sub 7 Kelvin to conform with Pb's critical temperature T_c.

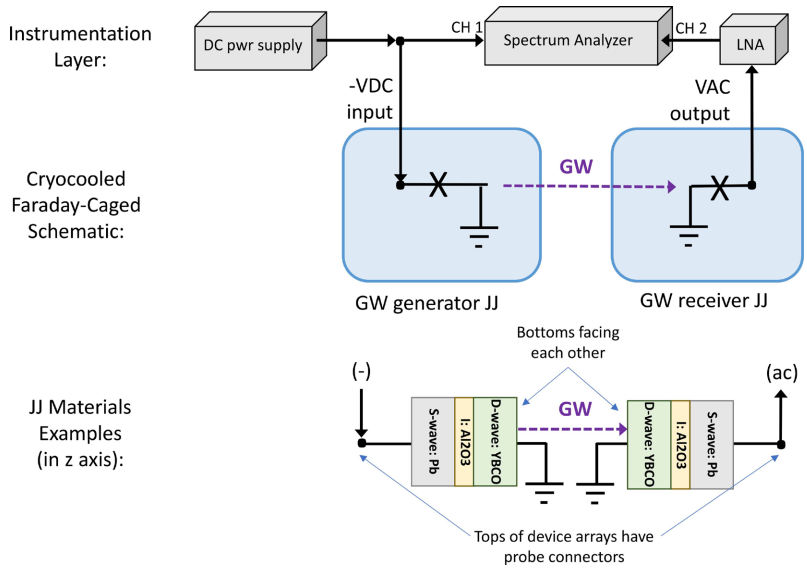

Figure 7. Josephson junction GW generation and detection lab setup.

The problem will be treated in two parts: emitted power estimates are made in 5.3.1, and detection sensitivity estimates are made in 5.3.2.

5.3.1. Emitted Power Estimates

For emitted power estimates we leverage the prior work done by Fontana [3], which estimated the power output for a Pb/BSCCO GASER. In the present paper, Pb/YBCO junctions are proposed. BSCCO and YBCO are both prominent d-wave high-temperature superconductors, with BSCCO offering higher critical temperatures around 90 - 110 K compared to YBCO's ~93 K. However, YBCO generally excels in practical applications due to superior critical current density (J_c) and manufacturability [18]. The band gaps of the two material selections are nearly the same, so their power output performance for the present paper will be taken as nearly equivalent.

Leveraging Ford's quantum approach [4] Fontana [3] derived the expected performances of a BSCCO HTSC GASER as summarized in **Table 4**. Fontana's device under analysis was a high-power bulk design, whereas in the present paper we have a low power thin film device, so it will be necessary to scale Fontana's results to fit the thin film constraints.

Table 4. Expected performance of bulk BSCCO HTSC GASER [3] (reprinted with permission).

Parameter	Value	Units
Energy of s/d wave gap in BSCCO	~1.3	THz
Power output with 10 kA/cm^2	~10	W/cm^2
Power output for multilayer	~10^3	W/cm^2
Volumetric Power Output	~10	MW/m^3

We note here that for the bulk device described in [3] that a current input of 10 kA/cm^2 is predicted to produce 10 W/cm^2, *i.e.* 1 A/cm^2 is expected to produce 1 mW/cm^2. How are we to scale this to a thin film Pb-YBCO device? While the current-voltage characteristic 'IVC' of Josephson Junctions (JJ) is a matter of detailed research [18]-[21], it is generally accepted that the critical voltage V_c, at which the JJ loses its superconducting properties, will be related to the critical current times the normal state resistance: $V_c = I_c \times R_n$.

Why normal state resistance? Because our JJ's will be biased with the DC current required to create the AC Josephson effect frequencies prescribed in **Table 1**, a nearly zero superconducting resistance of the junctions will necessarily result in the critical current I_c being exceeded, thus triggering normal state resistance R_n. The Resistance-Area product RA is typically given as: $RA = R_nA = 10^2 - 10^3\ \Omega\cdot\mu m^2$, so that for a emitter pad sized to a diameter of 3.1 mm, as shown in **Figure 6(a)** and **Figure 6(b)** one would then divide the RA product by the area $A_e = \pi(3.1\ mm)^2$, or $\pi(3100\ \mu m)^2 = 30{,}190{,}000\ \mu m^2$. For the high end of RA this leads to a per emitter resistance estimate of 33 μΩ per (17):

$$R_e = \frac{RA}{A_e} = \frac{10^3\ \Omega \cdot \mu m^2}{30190000\ \mu m^2} = 33\ \mu\Omega \tag{17}$$

With a bias voltage specified in Table 1 of roughly 50 μV, the expected bias current per emitter will be $I_b = V_b/R_n$ = 50 μV/33 μΩ = 1.5 Amps. 1.5 Amps emitted from an area of 0.3019 cm^2 results in ~5.0 Amps/cm^2 of emitter current density, resulting in a gravitational wave output, based on the ratios of Table 4, of approximately 5.0 mW/cm^2 of GW output per emitter. Multiplying by the emitter area A_e = 0.3019 cm^2 yields 1.5 mW of GW power per emitter. Returning to Figure 6(a) and Figure 6(b), one readily observes that the 150 mm array will result in a GW output power of 1.5 mW × 81 = 121.5 mW, whereas the 200 mm array will result in a GW output power of 1.5 mW × 129 = 193.5 mW. See Table 5 for a summary.

Table 5. Expected performance of thin film YBCO HTSC GASER.

Parameter	Value	Units
Power emitted per unit area	~5.0	mW/cm^2
Power output of one emitter	~1.5	mW
Power output for 150 mm array	~121.5	mW
Power output for 200 mm array	~193.5	mW

5.3.2. Detection Sensitivity Estimates

NEP of DJJs

In detection applications the sensitivity of a device is limited by its Noise Equivalent Power (NEP). In the context of detection, Dissimilar Josephson Junctions (DJJs) are more commonly known as 'Superconducting Tunnel Junctions, or STJs. [22] For YBCO NEPs of 10^{-15} to 6×10^{-2} $W/\sqrt{Hz}$ have been reported [23] [24]. Holdengreber (2018) [25] goes on to observe that the energy gap of YBCO permits signal detection up into the THz range, therefore our target frequency of 24 GHz as identified in Table 1 should not pose any difficulty in the way of detection. At a bandwidth of 10,000 Hz NEP would be on the order of 600 pW, resulting in a signal to noise power ratio (SNR) of at least 202.5(10)^6 for the 150 mm array, or better than a power ratio of 83 dB, assuming nearly perfect quantum conversion efficiency per (18):

$$\text{SNR} = \frac{\text{Power}}{\text{NEP}} = \frac{121.5\ \text{mW}}{600\ \text{pW}} = 202.5(10)^6 \approx 83\ \text{dB} \tag{18}$$

Quantum Efficiency of DJJs

The d-wave to s-wave conversion efficiency needed for a graviton to photon(s) conversion process is not well understood but is likely a function of quantum measurement efficiency [26] and doping profiles [27]. A range of doping regimes is recommended for experimental use to validate the best approach to enabling d-wave to s-wave graviton to photon(s) conversion. Given the small NEP cited in the proceeding analysis, even a small fractional quantum efficiency should result in an easily measurable signal.

5.4. Next Steps

For DJJs, a range of doping regimes was recommended in 5.3.2 to optimize band matching, for enabling d-wave to s-wave graviton to photon(s) conversion. In the event a link budget is established successfully, such a test rig could be extended to testing for potentially gravitomagnetically active materials as described in Stephenson [28] [29].

While not in the scope of this paper, other approaches to the generation and detection of gravitational radiation abound and bear mentioning here. The work of Gorlik *et al.* (2018) [30] is certainly at the forefront, outlining a method using intensive electromagnetic irradiation of high index dielectric materials.

An entirely unrelated technique using pairs of Josephson Junctions in an oscillatory regime has been proposed by Atanasov [31] [32] and may provide a parallel path worth investigating.

Recent fundamental research into YBCO may also yield additional benefits. Tahir-Kheli *et al.* [27] investigated using unique doping profiles to stimulate an s-wave YBCO phase at T_c's as high at 70 K, with a d-wave YBCO phase occurring in the same material at 100 K. If true, "then there is enormous value to current magnet technologies in uncovering this s-wave phase of YBCO" [27]. Relevant fundamental research into high-temperature cuprate superconductors is also evidenced in Yung-Yeh Chung [33], where operating near the quantum critical point may give rise to coherent behavior in quasi-particles potentially useful for spin-2 transition stimulation.

Finally, should the generation and detection of gravitational waves in a laboratory setting ever meet with success, the next logical question will be how to leverage gravitational wave technology for the application of propulsion. Concepts for GW propulsion are treated at a high level in Fontana's 2012 JSE paper [34], and would bear revisiting, should success ever befall this field.

6. Conclusion

An approach for developing, building, and testing phased array emitters of gravitational wave energy has been outlined using specially prepared Josephson Junctions. The remaining work is for the described hardware to be built and tested.

Acknowledgments

The author gratefully acknowledges helpful discussions with Eric Davis, Andrew Beckwith, Christian Corda, Giorgio Fontana, William Rieken, David Rossi & Kyle Gustin of Phase Helix, and Gurken Sufi & Yusha Bey of Ravata Solutions.

Conflicts of Interest

The author declares no conflicts of interest regarding the publication of this paper.

References

[1] Overduin, J.M. and Plendl, H.S. (2006) Leopold Ernst Halpern and the Generalization of General Relativity. https://arxiv.org/pdf/gr-qc/0608129

[2] Halpern, L. and Laurent, B. (1964) On the Gravitational Radiation of Microscopic Systems. *Il Nuovo Cimento*, **33**, 728-751. https://doi.org/10.1007/bf02749891

[3] Fontana, G. (2012) High Temperature Superconductors as Quantum Sources of Gravitational Waves: The HTSC GASER. In: Modanese, G. and Robertson, G.A., Eds., *Gravity-Superconductors Interactions*: *Theory and Experiment*, Bentham Science Publishers, 58-73.

[4] Ford, L.H. (1982) Gravitational Radiation by Quantum Systems. *Annals of Physics*, **144**, 238-248. https://doi.org/10.1016/0003-4916(82)90115-4

[5] Grishchuck, L.P. and Sazhin, M.V. (1973) Emission of Gravitational Waves by an Electromagnetic Cavity. *Zhurnal Eksperimental'noi i Teoreticheskoi Fiziki*, **65**, 441-454. http://jetp.ras.ru/cgi-bin/dn/e_038_02_0215.pdf

[6] Kiefer, C. (2025) Quantum Gravity. 4th Edition, Oxford University Press.

[7] Bishop, N.T., Kakkat, V., Kubeka, A.S., *et al.* (2024) The Interaction of Gravitational Waves with Matter. arXiv: 2405.07743. https://doi.org/10.1142/S0218271824410128

[8] Giorgio, F. (2012) High Temperature Superconductors as Quantum Sources of Gravitational Waves: The HTSC Gaser. https://www.researchgate.net/publication/286619454_High_temperature_superconductors_as_quantum_sources_of_gravitational_waves_The_HTSC_gaser

[9] (2025) Massachusetts Institute of Technology 6.763 2003 Lecture 11, AC Josephson Effect. https://web.mit.edu/6.763/www/FT03/Lectures/Lecture11.pdf

[10] (2025) US Amateur Microwave Bands Reference. https://rrra.org/post/2017/08/05/an-inexpensive-introduction-to-10ghz-microwave/#footnotes

[11] (2025) Wafer Electronics Sizes. https://en.wikipedia.org/wiki/Wafer_(electronics)#cite_note-f450c-13

[12] Moßle, M. and Kleinerm, R. (1999) c-Axis Josephson Tunneling between $Bi_2Sr_2CaCu_2O_{8+x}$ and Pb. *Physical Review B*, **59**, 4486-4496.

[13] Horng, H.E., Wang, L.M., Yang, S.Y., *et al.* (2000) Superconducting Pairing Symmetry in $YBa_2Cu_3O_{7ix}$ from a Study of Josephson Tunnel Junctions. *Chinese Journal of Physics*, **38**, 262-267.

[14] Physics Today (2005) High-Temperature Cuprate Superconductors Get to Work. https://physicstoday.aip.org/features/high-temperature-cuprate-superconductors-get-to-work

[15] MacManus-Driscoll, J.L. and Wimbush, S.C. (2011) Future Directions for Cuprate Conductors. *IEEE Transactions on Applied Superconductivity*, **21**, 2495-2500. https://doi.org/10.1109/tasc.2010.2100343

[16] Shen, T., Zlobin, A.V. and Larbalestier. D. (2022) White Paper on High Temperature Superconducting Bi-2212 Magnets for Energy Frontier Circular Colliders. *Proceedings of the US Community Study on the Future of Particle Physics* (*Snowmass* 2021), Seattle, 17-26 July 2022, C21-07-11.

[17] Wikipedia (2025) List of Superconductors (Element Portion). https://en.wikipedia.org/wiki/List_of_superconductors

[18] Lyatti, M., Gundareva, I., Röper, T., *et al.* (2024) Quantum Size Effects in Ultra-Thin $YBa_2Cu_3O_{7-x}$ Films. *Scientific Reports*, **14**, Article No. 221740.

[19] Kouznetsov, K.A., Sun, A.G., Chen, B. *et al.* (1997) C-Axis Josephson Tunneling Between $YBa_2Cu_3O_{7-\delta}$ and Pb: Direct Evidence for Mixed Order Parameter Symmetry in a High-T_c Superconductor. arXiv: cond-mat/9705283. https://arxiv.org/pdf/cond-mat/9705283

[20] Gu, Q., Wan, S., Tang, Q., Du, Z., Yang, H., Wang, Q., *et al.* (2019) Directly Visualizing the Sign Change of D-Wave Superconducting Gap in $Bi_2Sr_2CaCu_2O_{8+\delta}$ by Phase-Referenced Quasiparticle Interference. *Nature Communications*, **10**, Article No. 1603. https://doi.org/10.1038/s41467-019-09340-5

[21] Ohkubo, M., Uehara, G., Beyer, J., Mimura, M., Tanaka, H., Ehara, K., *et al.* (2022) Standard Measurement Method for Normal State Resistance and Critical Current of Resistively Shunted Josephson Junctions. *Superconductor Science and Technology*, **35**, Article ID: 045002. https://doi.org/10.1088/1361-6668/ac4f3b

[22] ESA Website (2019) Superconducting Tunnel Junction (STJ). https://sci.esa.int/s/wxDBYEw

[23] Rogalski, A. and Sizov, F. (2011) Terahertz Detectors and Focal Plane Arrays. *Opto-Electronics Review*, **19**, 346-404. https://doi.org/10.2478/s11772-011-0033-3

[24] Grimes, C.C., Richards, P.L. and Shapiro, S. (1968) Josephson-Effect Far-Infrared Detector. *Journal of Applied Physics*, **39**, 3905-3912. https://doi.org/10.1063/1.1656873

[25] Holdengreber, E., Moshe, A.G., Mizrahi, M., Khavkin, V., Schacham, S.E. and Farber, E. (2018) High Sensitivity High T_c Superconducting Josephson Junction Antenna for 200 GHz Detection. *Journal of Electromagnetic Waves and Applications*, **33**, 193-203. https://doi.org/10.1080/09205071.2018.1535333

[26] Macklin, C., O'Brien, K., Hover, D., Schwartz, M.E., Bolkhovsky, V., Zhang, X., *et al.* (2015) A Near-Quantum-Limited Josephson Traveling-Wave Parametric Amplifier. *Science*, **350**, 307-310. https://doi.org/10.1126/science.aaa8525

[27] Tahir-Kheli, J., Hlasek, T., Lojka, M., *et al.* (2023) Potential Major Improvement in Superconductors for High-Field Magnets. arXiv: 2304.06171. https://arxiv.org/abs/2304.06171

[28] Stephenson, G.V., Rieken, W. and Bhargava, A. (2019) Extended Cases of Laboratory Generated Gravitomagnetic Field Measurement Devices. *Journal of High Energy Physics, Gravitation and Cosmology*, **5**, 375-394. https://doi.org/10.4236/jhepgc.2019.52021

[29] Stephenson, G.V. (2021) High Index SMES Device for Gravitomagnetic Field Generation. *Journal of High Energy Physics, Gravitation and Cosmology*, **7**, 367-376. https://doi.org/10.4236/jhepgc.2021.72020

[30] Gorelik, V.S., Pustovoit, V.I., Gladyshev, V.O., Morozov, A.N., Kauts, V.L., Sharandin, E.A., *et al.* (2018) Generation and Detection of High Frequency Gravitational Waves at Intensive Electromagnetic Excitation. *Journal of Physics: Conference Series*, **1051**, Article ID: 012001. https://doi.org/10.1088/1742-6596/1051/1/012001

[31] Atanasov, V. (2019) Gravitational Wave Emission from Quadrupole Josephson Junction Device. arXiv: 1909.01732. https://arxiv.org/pdf/1909.01732

[32] Atanasov, V. and Saxena, A. (2023) Rapid Mass Oscillations for Gravitational Wave Emission: Superconducting Junctions. arXiv: 2307.00503. https://arxiv.org/abs/2307.00503

[33] Chang, Y., Van Nguyen, K., Remund, K. and Chung, C. (2025) A Mechanism for Quantum-Critical Planckian Metal Phase in High-Temperature Cuprate Superconductors. *Reports on Progress in Physics*, **88**, Article ID: 048001. https://doi.org/10.1088/1361-6633/adc330

[34] Fontana, G. (2012) Directions for Gravitational Wave Propulsion. *Journal of Space Exploration*, **1**, 8-16. https://www.tsijournals.com/articles/directions-for-gravitational--wave-propulsion.pdf

Nomenclature

The following nomenclature was utilized in the present work:

Section 1.0 nomenclature

$\mathcal{Y}_{J,l,M}^{\theta,\varphi}$	=	spinor coupling spherical harmonic tensors
$\ddot{\omega}$	=	spin eigenvectors
$\ddot{\omega}_M$	=	spin potential
$\ddot{\omega}_{\mp 2}$	=	spin 2 amplitudes
J, l, M, μ	=	quantum indices
θ, φ	=	angular indices
$\vec{\mathrm{q}}$	=	EM radiation potential

Section 2.0 nomenclature

$\overline{h_{\mu\nu}}$	=	metric perturbation
$\overline{h_{\mu\nu}^{in}}$	=	in-field metric component
$G_r\left(X, \dot{X}\right)$	=	retarded Green's function
$T_{\mu\nu}\left(\dot{X}\right)$	=	energy momentum tensor
$T_{\alpha\beta}\left(\ddot{X}\right)$	=	energy momentum tensor perturbation
$P = P_{sc}$	=	semi-classical radiated power
P_q	=	quantum case radiated power
$\lceil z \rceil$	=	resonant cavity dimension
ε	=	average energy density in the cavity
ω	=	radiating frequency
ℓ	=	characteristic cavity dimension
α	=	scaling constant, where $(\omega\ell)^{-\alpha}$ is mode function
β	=	quantum scaling constant
n	=	number of quantum radiators

Section 3.0 nomenclature

Γ_g	=	graviton transitions
Γ_e	=	electromagnetic dipole transitions
$P =$		emitted GW power
$P_p =$		Planck power ~ 10^{-5}g/10^{-44}sec - 10^{60} ergs/sec
ω	=	emitted frequency
ω_p	=	Planck frequency ~10^{44}/sec
$n =$		number of quantum emitters

Section 4.0 nomenclature

$V_0 =$	DC supply voltage
$v =$	AC Josephson effect voltage
$i =$	AC Josephson effect current
$I_c =$	DC level of critical current
$f_j =$	Josephson effect frequency
$\Phi_0 =$	Josephson effect wavelength
$\phi(t) =$	AC phase
$\phi(0) =$	initial phase
$\Omega =$	Ohms, units of resistance
$T_c =$	critical temperature
$J_c =$	critical current density
$V_c =$	critical voltage
$I_b =$	emitter bias current
$V_b =$	emitter bias voltage
$R_n =$	normal state resistance
$R_e =$	emitter resistance
$A_e =$	emitter area
NEP =	noise equivalent power
$\mathrm{W}/\sqrt{\mathrm{Hz}} =$	Watts per root Hertz (units of NEP)
SNR =	signal to noise ratio